Journal of Membrane Science 428 (2013) 52–62

Contents lists available at SciVerse ScienceDirect

Journal of Membrane Science

journal homepage: www.elsevier.com/locate/memsci

Gas transport through cork: Modelling gas permeation based on the morphology of a natural polymer material

Carla Brazinha [a,*], Ana P. Fonseca [b], Helena Pereira [c], Orlando M.N.D. Teodoro [b], João G. Crespo [a]

[a] REQUIMTE/CQFB, Department of Chemistry, FCT, Universidade Nova de Lisboa, P-2829-516 Caparica, Portugal
[b] Center for Physics and Technological Research, CEFITEC, Physics Department, FCT, Universidade Nova de Lisboa, P-2829-516 Caparica, Portugal
[c] Centro de Estudos Florestais, Instituto Superior de Agronomia, Universidade Técnica de Lisboa, Lisbon, Portugal

ARTICLE INFO

Article history:
Received 6 April 2012
Received in revised form
15 October 2012
Accepted 15 October 2012
Available online 27 October 2012

Keywords:
Gas permeation
Cork
Natural polymers
Solubility
Knudsen transport
Solution–diffusion model

ABSTRACT

Natural polymers have been studied during the last years for the transport and separation of liquid and gas mixtures, in terms of solubility and permeability data, and their structure and mechanical properties have been characterised. However, no transport models have been reported, relating transport with the material morphology. Cork is a natural cellular material containing three structural polymers (suberin, lignin and polysaccharides). Cork is considered a natural polymer, with economic relevance due to its sealing, non-toxic, stable and low-density properties. Cork was characterised in this work in terms of its solubility and permeability data in relation to various gases with different molecular mass: He, O_2, N_2, CO_2 and 1,1,1,2-tetrafluoroethane (R134a). A morphological analysis of the structure of the cork sample chosen in this work was also performed using SEM (scanning electron microscopy) and TEM (transmission electron microscope) image analysis, which took into account the variation of each relevant structural parameter.

A transport model was developed supported on the morphology of cork characterised in this work. The transport model developed considers that gas permeation occurs through the plasmodesmata, which are channels with approximately 100 nm of diameter that cross the cell walls of the cork cells. It was found that gas transport follows a Knudsen mechanism, as proved by the gas permeability behaviour with increasing gas molecular mass, with a negligible contribution of viscous transport to the total flux.

© 2012 Elsevier B.V. All rights reserved.

1. Introduction

The use of natural polymers has increased significantly in recent years, encouraged by their reduced ecological footprint and sustainability. This interest has been also extended to their use as membrane materials and thin films. In particular, cork has attracted attention since it is a renewable and sustainable raw material that has been used for many centuries. Its gas permeation properties and thermal insulation potential are also responsible for the commercial interest in this biomaterial.

Cork is a natural material that is obtained from the outer bark of the cork oak tree. The cork oak (*Quercus suber* L.) is a common oak species in Iberian Peninsula and the most important one in the oak open forests of the western Mediterranean region [1,2]. The natural cork business plays a key role in western European Mediterranean countries [3,4], with a cork oak area of 2.3 million hectares and a yearly average cork production of 374 000 t [5]. In particular, cork has a very high importance for Portugal because the country is the major world producer of cork products [3] and together with Spain represents 54% of the total area of cork oaks [5]. Although wine stoppers gave the cork oak world reputation, cork is also used for many other products or uses: sealing gaskets, heat and sound insulators and decorative uses, as well as composites [6]. The use of cork in these various applications is due to its appealing group of features, specifically low values of density, permeability and energy transfer coefficients, with a significant elastic behaviour and high physical, chemical and biological stability [3].

The characterisation of cork in terms of its sealing properties is extremely useful for practical reasons mainly related to wine aging, sealing gaskets and insulators. Literature reports several studies of oxygen mass transport through cork, more specifically through natural cork stoppers, in comparison with technical/synthetic corks and screw caps. These studies are often performed using wine-containing bottles [7–10] and the determined parameter is the oxygen transfer rate, *OTR* [mg(O_2)/stopper/year]. Unlike permeability, which exclusively depends from the intrinsic properties of the membranes, *OTR* depends also on the thickness of the material and on the driving force. Gas solubility in cork was also studied focused on the solubility of SO_2 [11].

The characterisation of cork in terms of its physical and mechanical properties [3,4], chemical composition [3,6] and morphology [3,4,13–15] has been published. Cork has a cellular

* Corresponding author. Tel.: +35 12 12948385; fax: +35 12 12948550.
E-mail address: c.brazinha@fct.unl.pt (C. Brazinha).

0376-7388/$ - see front matter © 2012 Elsevier B.V. All rights reserved.
http://dx.doi.org/10.1016/j.memsci.2012.10.019

structure with small, empty, closed cells with a hexagonal prism shape forming a highly ordered honeycomb [3,4,8]. The cell walls are very thin, with no intercellular spaces [3]. The major structural component is suberin, which together with lignin and polysaccharides make up the cell wall, while a significant amount of extractable material is also included [16,17]. Although natural cork has a regular cell structure [15,16], a large diversity of structural parameters is commonly observed.

Little attention has been given to the ultrastructure of cork cell walls. The cork cells do not have communicating features such as the pits that occur in wood cells, but they have the remains of the communication paths connecting physiological active cells, the so-called plasmodesmata. The plasmodesmata are present in the cell walls of cork, although not uniformly distributed, exhibiting a cylindrical form with a diameter of approximately 100 nm, filled after cell death with residues of proteins, phenolic compounds and other materials forming a less compact, non-structured matrix [4].

This work aims at understanding the mechanism of gas transport through cork, identifying the relevance of solubility and diffusion phenomena, and establishing a relation between the structural/morphological characteristics of the material and the resulting transport properties. In order to achieve this goal, a detailed characterisation of the cork material had to be acquired through scanning electron microscopy (SEM) and transmission electron microscopy (TEM), together with solubility and permeability studies using a series of gases with different molecular masses (He, N_2, O_2, CO_2 and 1,1,1,2-tetrafluoroethane (R134a). This structure/function approach has not been developed for studying transport through natural materials. A transport model supported on this approach is expected to contribute for the understanding of the underlying phenomena, opening also perspectives for the use of identical methodology for studying gas transport in other complex natural polymeric materials.

2. Experimental

2.1. Materials

The cork material used in this work was a reproduction cork (''Amadia'') type with a 9-year production cycle, suitable for cork stoppers, provided by the cork stopper company Cork Supply, Portugal. The cork was taken from planks with an average 38 mm of thickness previously boiled in water during 1 h and air dried for 2–3 days. Boiling is a typical treatment performed to cork in order to expand and to straighten the cell walls, and hence obtaining a more uniform cell structure without significant changes in its chemical composition [18]. Moreover, the boiled cork shows lower values of gas permeability [16], which is desired from an application point of view. All the wine cork stoppers are produced using water boiled cork planks.

The same cork sample was used in all permeability experiments performed and cell structure measurements obtained from SEM and TEM image analysis. A disk with 2 mm thickness and an effective diameter of 3.5 mm was used in these studies. This sample was cut in a way that the gas crossed the cork disk as on natural cork stoppers, meaning that the circular sections were transverse sections of cork and the gas flow was in an axial direction of cork [19]. Furthermore, the sample chosen had no macroscopic holes (*i.e.,* lenticular channels) and it was weighted prior to each experiment. For the solubility experiments, cork was taken from the same cork plank, and hence, from the same material used on the permeability measurements. Cork was milled using a knife mill (Retsch SM 2000) with an output sieve of $2 \times 2\ mm^2$ and screened using a vibratory sieving apparatus (Retsch AS 200 basic).The cork sample prepared had a granulometry of 1–2 mm.

Non-condensable gases with various molecular masses were studied in this work: helium (Air Liquide), nitrogen (Air Liquide), oxygen (99.999%, Praxair) and carbon dioxide (SFE 99.998%, Praxair) were used. Additionally, the refrigerant gas R134a (Air Liquide), with a molecular weight of 102 g/mol, was also used.

2.2. Experimental procedure

2.2.1. Characterisation of the cork cell structure

The cork cell structure of the upstream, downstream and cross-sectional surfaces of the cork disk under study was characterised by scanning electronic microscopy (JEOL-JSM-840) using an acceleration voltage of 25 kV, after coating the cork disk with gold under vacuum conditions (layer with approximately 200 Å of thickness), as can be seen in Fig. 1.

The dimensions of the cork cells were obtained by using an image analysis system with a camera CCD-IRIS/RGB on a Kaiser RS1 table with manual light control and by using the Analysis® *vs* 3.2 software program. The prism lateral length of the cork cell, l (μm), and the diameters of the prism bases at half lateral length were measured on 5 points uniformly distributed on the sample, by measuring 30 cork cells per point on the upstream and downstream circular surfaces. On the cross section surface measurements of two crossed diameters (μm) of the prism bases (d_{height} and d_{width}) were made.

The plasmodesmata were characterised using a transmission electron microscope (JEOL JEM-100SX) with an acceleration voltage of 80 kV, after cutting transverse ultra-thin sections (~700 Å) using a diamond knife and stained with uranyl acetate for 5 min and lead citrate for 15 min. The negatives of the images acquired were scanned, as shown in Fig. 2.

2.2.2. Density of the cork material

The density of the boiled natural cork used was 168 kg/m^3. The density of the natural cork used was determined from the weight and the volume of the correspondent cork plank after being dried in an oven.

2.2.3. Permeability experiments

Helium was selected as a reference gas when preparing and optimising the permeability experiments procedure. Helium has been previously used in a detailed study where the variability of gas permeation using more than one hundred samples from different cork plank qualities was assessed [20].

For measuring helium permeabilities, after placing the cork disc in the sample holder, a Helium mass spectrometer leak detector (type ASM 142 from Adixen) was connected to the downstream compartment of the holder and the upper and lower volumes were pumped down to pressures below 0.1 mbar. Then, the upper part was filled with 1 atm of pure helium, measured by a pirani–piezo gauge (models VSC42MA4 and VSP52MA4, Thyracon). To assure that this pressure was kept constant, a fine valve connected to the gas was used. The volumetric flow-rate of the gas i through the cork disk, $Q_{vol,i}$ [$Pa\ m^3\ s^{-1}$], was recorded by connecting the leak detector directly to the computer. The experiment was performed for a time long enough to obtain a stable value of $Q_{vol,i}$, and hence ensuring steady-state conditions [20].

To perform the permeability tests, a sample holder was specially constructed. The cork piece was tightened between the holder body and a screwable cylinder, both having a drilled aperture of 3.5 mm in diameter. The holder was fitted with two standard KF25 flanges for an easy mounting in the leak detector and the pressure rise system. To assure that every sample was

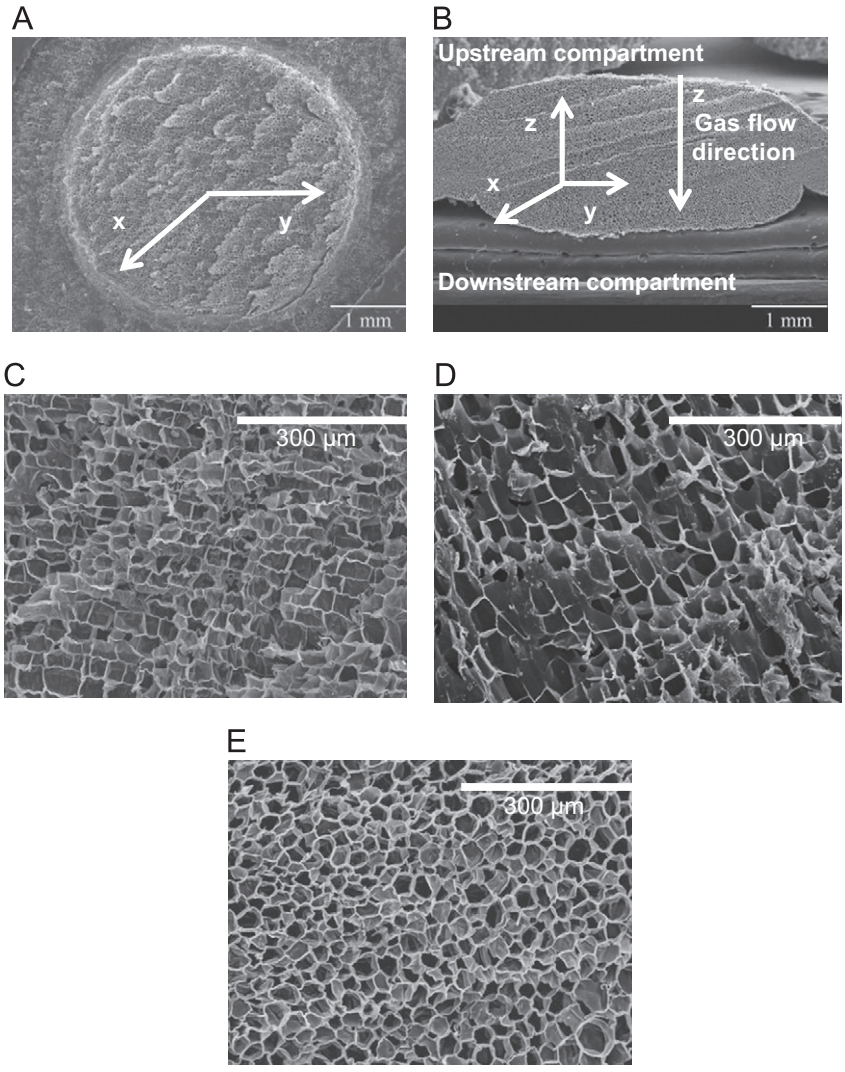

Fig. 1. SEM pictures showing the general aspect of the cork sample studied in this work: the upstream surface (Fig. 1A) and the cross-section surface (Fig. 1B). The *xy* surface corresponds to the surface perpendicular to the gas flow direction (*z*). Magnified SEM pictures of the cork sample: the upstream surface (Fig. 1C), the downstream surface (Fig. 1D) and the cross-section surface (Fig. 1E).

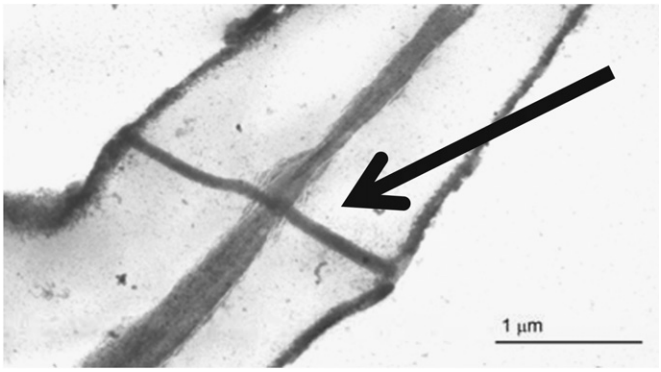

Fig. 2. TEM image of the wall of cork cells. A plasmodesmata is evidenced by the arrow in the image.

well sealed between the two surfaces and that the gas flow was only passing through the sampled area, the piece needed to be greased in the lateral surfaces every time a new sample was tested. The temperature of the holder was controlled by the use of a water bath and the temperature was measured with a calibrated thermocouple, at 23 ± 2 °C.

Before starting the permeation tests and once reaching the test temperature, the contribution of residual degassing to the pressure was measured. Then, the sample was tested with several non-condensable gases by this order: He, N_2, He, O_2, He, CO_2, He, R134a, and finally He. The helium permeability value was used as a reference and to check the sample status. The permeabilities of cork to the various gases were measured maintaining the upstream pressure constant at 1 atm.

Cork permeabilities to the various gases were measured using a rig with the scheme shown in Fig. 3. This system was composed by a high vacuum part, consisting of a rotary vane (E2M5, Edwards) and turbomolecular pumps (5080, Alcatel), where the downstream compartment was coupled to and evacuated to a pressure below 5×10^{-6} mbar. The downstream compartment was also connected to a high accuracy gauge (MKS 690A Baratron) used to monitor the rising pressure due to the passing gas through the cork. The upper part of the holder was also connected to the vacuum pump by a valve, to the gas bottle and to a pressure gauge (baratron 5 bar, MKS), which measured the feed pressure. The permeate pressure was monitored for long time enough to achieve a constant slope pressure increase, in order to assure steady-state conditions. Usually each gas permeability test had duration of one full day.

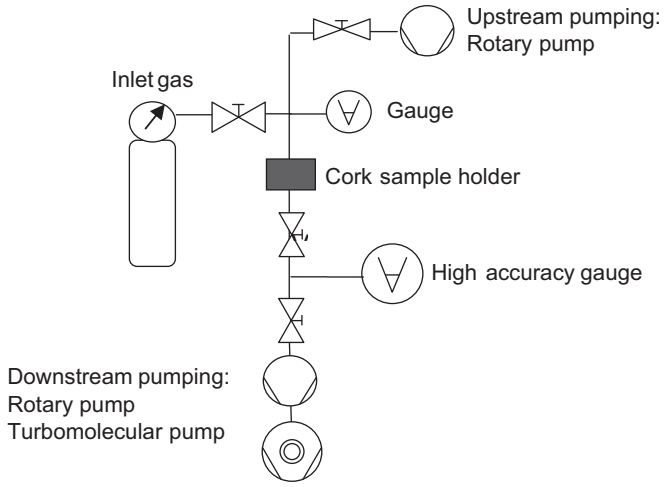

Fig. 3. Permeability test rig used for the pressure rise method. The lower volume is evacuated to a pressure below 5×10^{-6} mbar. The upper side volume is filled with the test gas. The pressure in the lower volume was monitored with a pressure gauge.

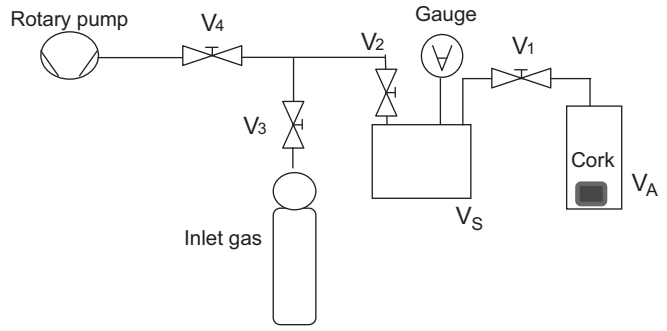

Fig. 4. Solubility rig. In the beginning of each solubility experiment, all valves are opened and both storage volume, V_S [m^3], and the absorption volume, V_A [m^3] are connected to pumping via V_1. Then valves V_1 and V_4 are closed and the storage volume V_s is filled by opening valve V_3. After reaching the test pressure, valves V_3 and V_2 are closed. When the pressure in the storage volume V_S is stable, valve V_1 is open.

For obtaining the permeabilities of cork to the various gases, using calculations from the gas volumetric flow-rates, it is necessary to determine accurately the volume of the permeate compartment, V_{perm}. For this purpose, different control volumes with a precisely known volume value, ΔV, were connected to the permeate volume and the corresponding permeate pressure, p_2, was measured. To ensure reliable results, the volume V_{perm} was measured several times, by an adiabatic expansion and compression and an average value was used. The equation used to calculate the volume of the permeate compartment was the Boyle's gas law, Eq. (1):

$$p_1 \times V_{\mathrm{perm}} = p_2 \times (V_{\mathrm{perm}} + \Delta V) \Leftrightarrow V_{\mathrm{perm}} = \frac{p_2 \times \Delta V}{p_1 - p_2} \quad (1)$$

where p_1 and p_2 are respectively the initial and final pressures measured. The value determined for V_{perm} was $(86.5 \pm 0.1) \times 10^{-6}$ m^3.

2.2.4. Solubility experiments

Fig. 4 shows a scheme of the unit used for the solubility experiments. The storage volume, V_S [m^3], and the absorption volume, V_A [m^3], were coupled by a valve and both connected to pumping. Then the volume V_A was filled with 2.00 ± 0.04 g of milled cork. Afterwards the following procedure was performed: (1) both volumes were pumped for at least 3 h; (2) the valve V_1 connecting V_S to V_A was closed and V_S was filled with the selected gas until a pressure of 2 bar was reached, except for helium where the value was 1.5 bar, due to problems in stabilising the pressure; (3) after reaching pressure stabilization (typically a few minutes), valve V_1 was opened and the gas expanded to both volumes; (4) the gas was absorbed by the cork causing a decrease on the pressure.

The pressure was monitored by a high accuracy pressure gauge (MKS 5000 mbar Baratron) until the pressure reached a stable value. The pressure was obtained after a minimum of 3 days stabilization time. The gauge was connected to an ADC-16 High Resolution Data Logger that was linked to the computer so the pressure data was monitored on-line and recorded. The unit was in a controlled temperature room; the temperature of the unit was measured by the use of a calibrated thermocouple and it was 23 ± 1 °C. Solubility tests were performed to 4 different gases: He, N_2, O_2, CO_2 and R134a. To calculate the amount of gas i absorbed by the cork, $n_{i,cork}$ [mol], the following relation was used:

$$n_{i,\mathrm{cork}} = \frac{p_0 \times V_S - p \times (V_S + V_A - V_{\mathrm{cork}})}{RT} \quad (2)$$

where p_0 (Pa) is the pressure test used to fill the storage volume, V_S [m^3], p [Pa] is the monitored pressure, V_C [m^3] is the cork volume, R [$J\,K^{-1}\,mol^{-1}$] is the ideal gas constant and T(K) is the temperature. In order to know the volumes V_S and V_A, the same procedure was followed as described previously for determining the volume of the permeate circuit. The values of V_S and V_A were respectively $(67.5 \pm 6.0) \times 10^{-6}$ m^3 and $(127.7 \pm 2.1) \times 10^{-6}$ m^3. The V_{cork} value was calculated from the mass of cork used and the density of 168 kg/m^3 obtained experimentally.

The solubility coefficient, S_i, expressed in (cm^3(STP))/(cm^3_{polymer} atm) units, which are commonly used when referring to the solubility of gases, is calculated respectively through Eq. (3):

$$S_i = \frac{V_{i,\mathrm{cork}}(\mathrm{STP})}{V_{\mathrm{cork}} \times p_{\mathrm{estabilised}}} \quad (3)$$

where $V_{i,\mathrm{cork}}$ (STP) [m^3], is the volume of gas i corresponding to $n_{i,\mathrm{cork}}$ at STP conditions (1 atm, 273.15 K), and $p_{\mathrm{estabilised}}$ [atm] is the pressure measured at equilibrium conditions.

3. Results and discussion

3.1. Cork structure

The analysis of the structure of the sample chosen for this work was performed by scanning electron microscopy. Fig. 1 shows the upstream surface (Fig. 1A) and the cross section surface (Fig. 1B) of the cork disk. The absence of lenticular channels or of other extraneous materials is confirmed, which attests the homogeneity of the chosen cork sample.

In general terms, the upstream, downstream and cross-section surfaces of this sample (respectively Fig. 1C–E) present a very uniform cork cell structure with the cells arranged very regularly in parallel rows without intercellular voids. As expected [15], the cells show on the transverse section of cork of the upstream and downstream surfaces a rectangular shape, with a "brick wall" arrangement, while in the cross-sectional surface that corresponds to a tangential section of cork cells appear with hexagonal form with a "honeycomb" arrangement. The image analysis of the cells shown in Fig. 1 allows determining the most relevant dimension parameters of the cork cells. The values obtained from the analysis of the working sample are in good agreement with the values reported in the literature [4,16] (Table 1A).

Table 1
Average characteristic dimensions of the cell structure of the cork sample used in the gas permeability measurements (upstream, downstream and cross-section surfaces): (A) obtained from SEM image analysis and (B) obtained from visual observation of TEM images.

	Upstream surface	Downstream surface	Cross-section surface
A.			
l [μm]	44 ± 12	55 ± 13	–
d_{width}[a][μm]	–	–	29 ± 8
d_{height}[b] [μm]	31 ± 7	32 ± 7	32 ± 9
δ_{wall} [μm]	–	–	$1.(5) \pm 0.(5)$ Cross section surface

B.	
Tortuosity of the plasmodesmata, $\tau_{plasmodesmata}$ [−]	1
Diameter of the plasmodesmata [nm]	100
Number of plasmodesmata per cork cell along the flux direction, $\overline{n}_{plasmodesmata}$[−],	3

l is the lateral prism length; and d_{width} and d_{height} are the diameters of the prism base, respectively perpendicular and along the gas flow direction. The wall thickness of the cork cell, δ_{wall}, and the parameters in Table 1B, were determined only in the tangential section of cork (corresponding to the cross section surface).

[a] Perpendicular to the gas flow direction.
[b] Along the gas flow direction (z).

Table 2
Young modulus for natural cork and synthetic polymers [25].

Material	E [MPa]
Polycarbonate	2000–2400
Polysulfone, PSU	~2500
PTFE, Teflon	410–750
Silicone Rubber, PDMS	1–5
Natural cork (alveolar cell structure)[a]	15–30 (non-radial direction) [12] 9.5–12.5 (radial direction) [14] 10–20 [16]
Material of the wall of the cork cell	~9000 [5,26]

[a] In the region of viscoelastic, with linearity between the stress and the strain for small deformation values of the material.

Fig. 2 shows a TEM image of cork cell walls, where plasmodesmata can be clearly visualised. As referred above, the plasmodesmata are channels that cross the cell walls and are filled with residues after cell dead. As exemplified in Fig. 2, visual observation of cell walls allows for determining the parameters of the plasmodesmata which are more relevant to the cork transport, as shown in Table 1B. The plasmodesmata are almost non tortuous and, therefore, a tortuosity, $\tau_{plasmodesmata}$ [−], of 1 was considered; they have a regular cylindrical form and a diameter of around 100 nm, in accordance with the values determined in [4]. The average number of plasmodesmata per cork cell, in the gas flux direction, $\overline{n}_{plasmodesmata}$ was considered to be in average equal to 3.

From TEM images, it was also observed that the plasmodesmata are filled with a material with a much lower density (darker region in Fig. 2) than the cell wall material (lighter area in Fig. 2). Despite the high flexibility of the natural cork as a whole, the wall of the cork cell is a highly rigid material with an extremely high value of the Young modulus (see Table 2) that strongly suggests that gas transport may be significantly hindered by such rigid material.

The subsequent analysis of the process of gas transport through natural cork will be supported in the assumption that gas transport through cork occurs through the plasmodesmata, neglecting any other contributions.

3.2. Permeabilities of non-condensable gases through natural cork

The volumetric gas flow-rate, $Q_{vol,i}$ [Pa m^3 s^{-1}] can be experimentally measured as described above (Eq. (4)) and the corresponding molar flow-rate of a gas i through natural cork, $Q_{molar,i}$ [mol s^{-1}] can be determined (Eq. (5)). If the cross section of the cork disk is known as well as its thickness, the permeability of natural cork to a defined gas i, P_i [mol m^{-1} s^{-1} Pa^{-1}], can be calculated knowing the driving force applied based on the pressure of gas i, Δp_i [Pa], using Eq. (6):

$$Q_{vol,i} = \frac{dp_i}{dt} \times V_{perm} \tag{4}$$

$$Q_{molar,i} = \frac{1}{RT} \times Q_{vol,i} \tag{5}$$

$$P_i = \frac{Q_{molar,i}}{A_{cork} \times \Delta p_i} \times \delta_{memb} = \frac{Q_{molar,i}}{A_{cork} \times \left(p_{i,feed} - p_{i,perm}\right)} \times \delta_{memb} \tag{6}$$

where V_{perm} [m^3] is the volume of the permeate circuit, A_{cork} [m^2] is the area of the cork disk and δ_{cork} [m] is the thickness of the cork disk. Permeabilities of natural cork to non-condensable gases expressed in mol m^{-1} s^{-1} Pa^{-1} units can be converted to m^2 s^{-1} units by multiplying the permeability by the perfect gas constant and the temperature.

In this work, the permeability of O_2 through this sample was found to be 2.8×10^{-14} kg (O_2) m^{-1} s^{-1} Pa^{-1} or 2.1×10^{-9} m^2 s^{-1} at 23 °C. The corresponding calculated value of oxygen transfer rate, *OTR*, is 129 mg (O_2) over one year, considering an oxygen composition of 21% in air at atmospheric pressure, a disk diameter of 20 mm and a thickness of 45 mm. These values are within the orders of magnitude of the range of values reported by Sanchez et al., of *OTR* of 400 to 2.56×10^5 mg over one year [21], namely in the low range of values as the sample chosen had no macroscopic holes, which in our case significantly contributed to a lower value of *OTR*.

In order to characterise natural cork in terms of type of polymer behaviour, its gas transport properties are compared with selected synthetic polymers reported in the literature. The selected polymers are used in gas and vapour separations and are similar to others used in sealing systems, a common application

of cork. With the purpose of covering a large range of situations, the behaviour of natural cork is compared with polymers with diverse viscoelastic properties, from glassy to rubbery polymers. Particularly, natural cork behaviour is compared to polycarbonate, PTFE (Teflon AF2400) and PDMS. The permeability of different gases through natural cork and also through the other selected polymers is plotted *versus* the Lennard–Jones diameter, d_{LJ} [Å], a molecular collision diameter, as shown in Fig. 5. Additionally, the modulus of elasticity, the Young modulus, E, a measurement of the stiffness of the material, is shown in Table 2.

The polymers chosen to be compared with cork follow the solution–diffusion model of transport, as mentioned in [22,23]:

$$P_i = S_i \times D_i \tag{7}$$

where S_i is the solubility coefficient of gas i and D_i [$m^2\ s^{-1}$] is the diffusion coefficient of the gas. Thus, permeability is determined by diffusion related to the size of the permeating species and by solubility related to affinity interactions between the membrane and the permeating species.

As expected, the permeability of different gases through PDMS membranes increases with the gas molecular weight or penetrant size (Lennard–Jones diameter). Since PDMS is a rubbery polymer, with a low value of the Young modulus, its ability to accommodate larger gases is high and solubility phenomena dominate the process of gas transport. Larger gases, such as carbon dioxide or propane, can establish intermolecular Van de Waals interactions with the polymer and solubility effects become more relevant [23].

On the contrary, the decrease of the permeability of gases with the increase of the gas molecular weight is typical for glassy polymers, with a high value of the Young modulus, in which gas transport is mainly controlled by diffusion phenomena. As a consequence, the selectivity observed for the transport of a particular gas in comparison with other(s), is mainly explained by the different diffusivity of gases through cork. This trend is typically observed in the case of rigid polymers with low-free-volume and low affinity to gases, such as polysulfone [27] and polycarbonate [22].

Teflon AF 2400, although being a polymer with a high free volume fraction of 32.7% was reported as having similar behaviour to rigid glassy polymers [22,28] (although the deviation reported for CO_2). In this work, a similar behaviour was observed for natural cork, which may not be expected due to its low density [3,8] and free volume, higher than 70% [16], associated to a high flexibility of the material as a whole and a low value of Young modulus. However, if the high value of the Young modulus of the cell walls of cork is considered, the trend observed might suggest a dense glassy behaviour.

3.3. Solubility of non-condensable gases in cork

In order to determine the solubility coefficients of gases in natural cork, the amount of each gas solubilised, $n_{i,\mathrm{cork}}$ [mol] (see Eq. (2)), was measured along time, as it is shown in Fig. 6.

The solubility coefficients in cork, calculated at equilibrium conditions, when the concentration of each gas reaches a constant value, and the solubility coefficients in PDMS and in PTFE (Teflon AF2400) are reported in Fig. 7. These polymers exhibit permeability values not significantly lower than the one measured for cork, which may suggest that cork behaves as a dense polymer. The values of the solubility coefficients are expressed in $(cm^3(STP))/\left(cm^3_{polymer}\ atm\right)$ units.

For each gas, the glassy PTFE polymer had higher solubility coefficients than the rubbery polymer PDMS, in line with the common tendency reported in literature [28]. Nevertheless, as is shown in Fig. 5, a polymer behaving as a glassy polymer is not sensitive to changes in permeability due to solubility (even if the value of the solubility coefficient is higher), unlike rubbery polymers [23,30]. For example, the permeability of propane, C_3H_8, is similar to nitrogen permeability in the case of the glassy PTFE but, in the case of the rubbery polymer PDMS, propane permeability is significantly higher than that of nitrogen (see Fig. 5), even though its solubility coefficient is lower (compared to PTFE) (see Fig. 7).

The very high Young modulus of the cork cells' walls and the higher values of solubility coefficients in cork than the values for a

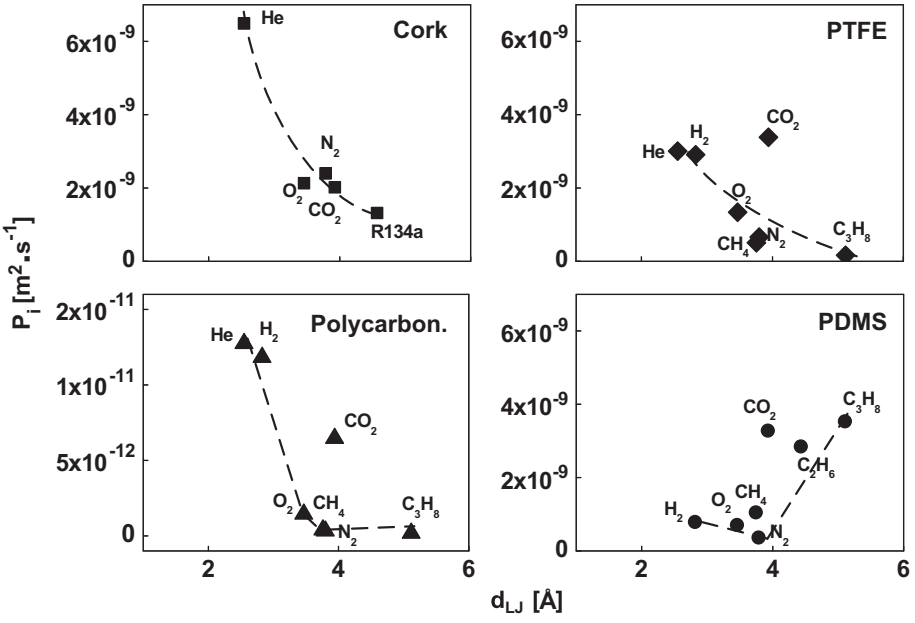

Fig. 5. Permeabilities of various gases, P_i [$m^2\ s^{-1}$], in natural cork (23 °C, 1 atm), in low free volume polycarbonate and in the high free-volume PTFE, Teflon AF 200 (25 °C, 3.4 atm) [22] and in PDMS (35 °C, 1 atm) [23], as a function of the Lennard–Jones collision diameter, d_{LJ}, expressed in Å (10^{-10}) [24]. Dashed lines are plotted only to guide the eye.

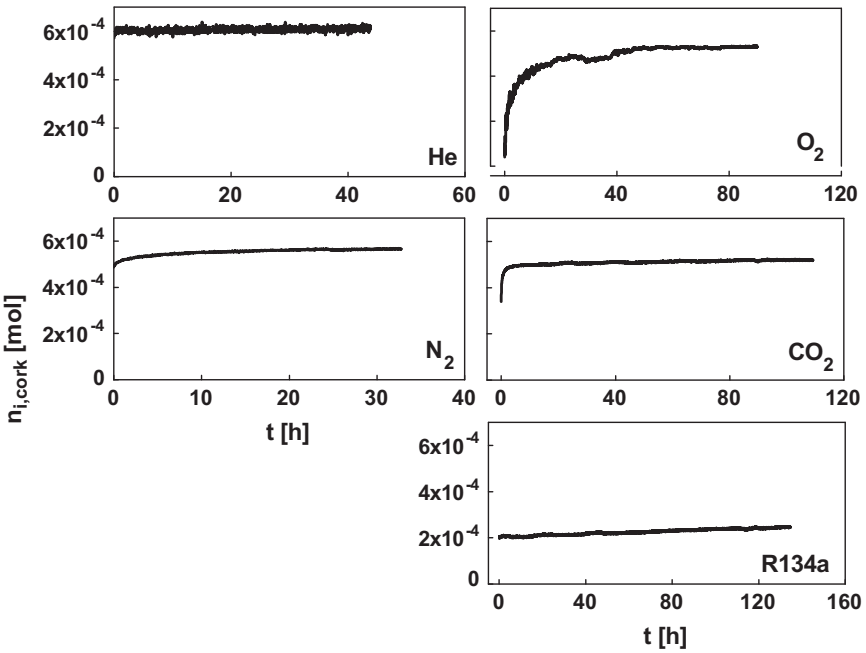

Fig. 6. Amount of each gas sorbed in cork, $n_{i,cork}$ [mol], (raw experimental data) at 23 ± 1 °C as a function of time. The gases studied were helium, oxygen, nitrogen, carbon dioxide and R134a.

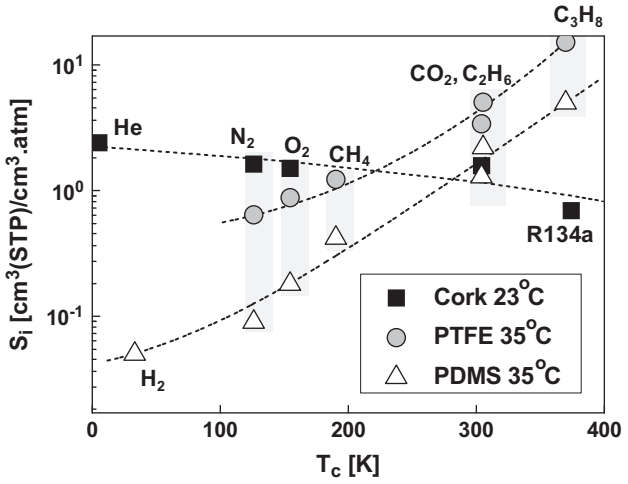

Fig. 7. Solubility coefficients of selected gases in natural cork, PDMS [23] and PTFE [28], S_i, expressed in $(cm^3(STP))/\left(cm^3_{polymer}\ atm\right)$ units, *versus* the critical temperature of the gases, Tc [29]. The dash trend lines added to the figure are a guidance to the eyes.

typical rubbery polymer (PDMS) might suggest a glassy behaviour for cork. However, the solubility coefficients in cork do not correlate with the critical temperature of the gases under study (which is related with the binding enthalpy between the gas and the polymer [31] and with the gas condensability [32]), as it is observed for glassy and rubbery dense polymers [30,31] (see Fig. 7). In fact, the solubility coefficients of gases in cork slightly decrease with the increase of the critical temperature, in total opposition with the behaviour observed in dense polymers.

3.4. Mechanism of gas transport through natural cork

From the sorption experiments, which results are shown in Fig. 6, the rate of gas penetration within cork (or the amount of each gas sorbed in cork, $n_{i,cork}$) was plotted *versus* the square root of time, during the transient response period, particularly for the initial instants. As it can be observed this relation is not linear for O_2 for initial periods of time higher than 540 s and higher than 120 s for CO_2. For the other gases studied the transient period was too short to be analysed. A linear relationship would be expected if the transport of these gases could be described by a Fickian diffusion law, typical in dense polymers [30].

Therefore, although cork presents low permeability towards different gases and could suggest a glassy polymer behavior, the non-increasing relation between critical temperature of gases and their solubility in cork and the non-fickian relation between solute penetration with time, clearly indicate that gas transport through cork should take into consideration its porous morphology presented above (see 3.1.). Considering the extremely dense and rigid character of the cell walls of cork it seems clear that gas transport may only occur through the plasmodesmata, even if these pores are not totally open, but partially filled with organic material.

Considering the existence of pores in cork responsible for gas transport (see 3.3.), it is important to know if gas permeates cork through a convective transport mechanism induced by the overall pressure difference across the cork material (Darcy law), or if permeation occurs through a Knudsen molecular diffusion mechanism, regulated by the difference in concentration (partial pressure) of a given gas across cork. In this later case the gas dynamics would be mainly explained by gas molecular collisions with the walls of the plasmodesmata. Fig. 8

In order to elucidate the driving force responsible for the gas transport through cork, the effect of the partial feed pressure of gas *i* and the effect of the total feed pressure on flux of gas *i* were assessed. The chosen gas for this experiment was helium, because the helium leak detector allows for measuring on-line the volumetric flow-rate of helium through cork (one-data point acquisition each 1 to 2 s), from which the on-line helium fluxes were calculated through Eq. (5). In order to increase the total feed pressure, without changing the partial pressure of He, nitrogen was used. In Fig. 9, the partial feed pressures of He and of N_2, the total feed pressure and the corresponding helium flux are presented along time. As it can be seen, the helium flux increased when the helium feed pressure increased but it remained constant

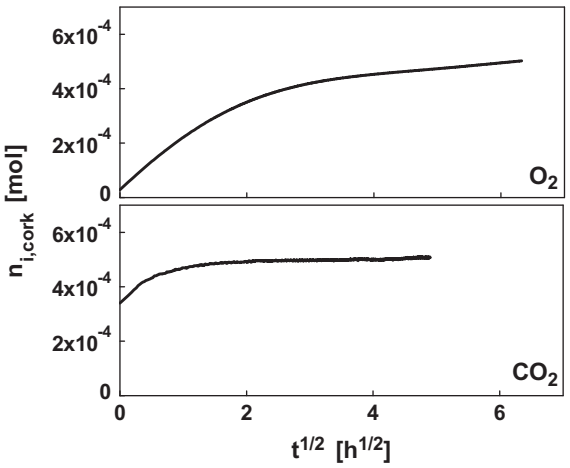

Fig. 8. Amount of oxygen and of carbon dioxide sorbed in cork, $n_{i,\mathrm{cork}}$ [mol], at 23 ± 1 °C as a function of the square-root of time, $t^{1/2}$ [$h^{1/2}$].

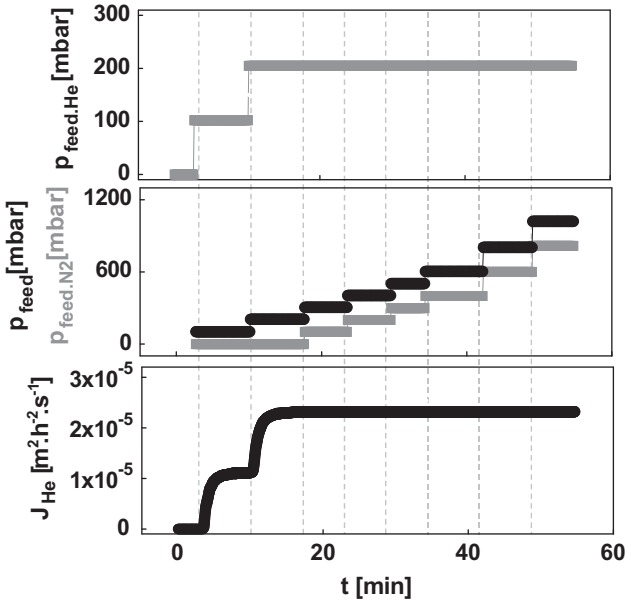

Fig. 9. Helium feed pressure, $p_{\mathrm{feed,He}}$ [mbar], total feed pressure, p_{feed} [mbar], nitrogen feed pressure, $p_{\mathrm{feed,N_2}}$[mbar] and helium flux through cork, J_{He} [mol m^{-2} s^{-1}] as a function of time. Obs.: Each vertical dash line in each figure corresponds to an increase of partial pressure of He or of N_2.

when the total feed pressure was varied by increasing of the pressure of nitrogen (with the helium feed pressure constant). This study shows clearly that gas transport through cork is regulated by the partial pressure (or concentration) of the gas under study, meaning that gas transport follows a diffusional transport mechanism.

Considering these results, the Knudsen number for each gas i, Kn_i [–] (see Eq. (8)) [33], was calculated by comparing the molecular mean free path of gas i, λ_i [m], with the average pore diameter of the material, d_{pore} [m].

$$Kn = \frac{\lambda_i}{d_{\mathrm{pore}}} \tag{8}$$

$$\lambda_i = \frac{k_B \times T}{\sqrt{2} \times \pi \times d_{LJ,i}^2 \times p} \tag{9}$$

where k_B [J/K] is the Boltzmann constant and p [Pa] is the gas pressure, considered to be the pressure of the gas i in the upstream compartment, p_{feed} [Pa].

The plasmodesmata, through which gas permeation takes place, have rather constant diameters (100 nm), measured by TEM. However, they are partially filled with organic material. Therefore, when calculating the Knudsen number for each gas for transport through cork, it was decided to assume an equivalent diameter of plasmodesmata ranging from 50 to 100 nm.

For Helium, which transport through cork was proven to clearly follow diffusional molecular flux (see Fig. 9), the calculated Knudsen numbers were 2.8 and 1.4, respectively when the effective pore diameter of cork, $d_{\mathrm{plasmodesmata}}$, was considered to be 50 and 100 nm. The other gases studied in this work have similar Knudsen numbers, so they also are expected to follow a diffusional transport type. Even in the case of the gas R134a (selected gas with the highest Lennard–Jones diameter), the Knudsen numbers are of 0.9 and 0.5, respectively when the $d_{\mathrm{plasmodesmata}}$, is 50 and 100 nm. These values support a typical Knudsen molecular flow regime (usually considered for Knudsen numbers higher than 0.5 [34]). Still, the contribution of viscous flow to the total flow may be also calculated (see Section 3.5).

Considering that gas transport takes place through a Knudsen diffusion mechanism, then the following formalism may be applied:

$$D_{\mathrm{eff},i}^{k} = \frac{\varepsilon \times d_{\mathrm{pore}}}{3 \times \tau} \times \left(\frac{8RT}{\pi M_i}\right)^{1/2} = K \times M_i^{-1/2} \tag{10}$$

where $D_{eff,i}^{k}$ [m^2 s^{-1}] is the Knudsen effective diffusivity of a gas i, ε [–] and τ [–] are, respectively, the porosity and the tortuosity of the permeating media, d_{pore} [m] is the pore diameter of the permeating media and M_i [g/mol] is the molecular weight of the gas i. K is a constant which exclusively depends on the permeating media and temperature.

Fig. 10 shows an excellent linear relation between the experimental diffusivities of the selected gases in cork and their $M_i^{-1/2}$, which is also a strong evidence that gas transport through cork follows a Knudsen molecular diffusion mechanism.

3.5. Modelling of gas permeation based on the morphology of natural cork

As referred to, the ultimate goal of this work is the establishment of a relation between the structural/morphological

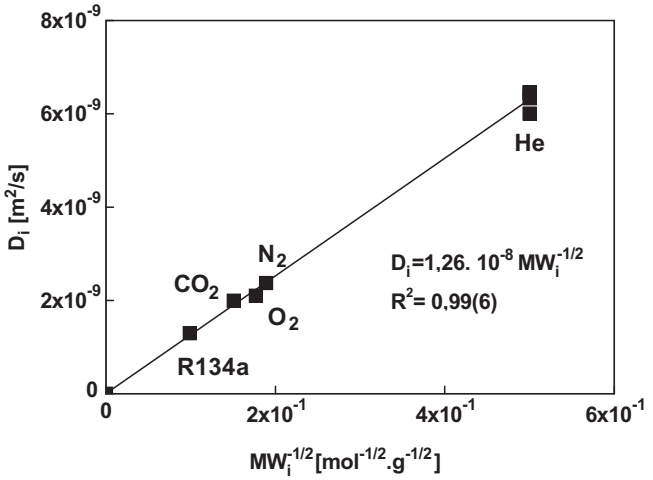

Fig. 10. Diffusivities of helium, nitrogen, oxygen, carbon dioxide and R134a in natural cork (23 °C, 1 atm) as a function of the molecular mass $M_i^{-1/2}$ of each gas i obtained in this work (in dots), with a linear fitting.

characteristics of the material and the resulting transport properties. In order to achieve this goal, a detailed characterisation of the cork material was performed. A transport model supported on this approach is developed in this section.

Based on the morphology of the cork sample studied and considering that gas transport follows a Knudsen diffusion behaviour, a transport model may be developed. The following assumptions were also considered:

(1) The cork cell structure is schematically shown in Fig. 11A–D. It was considered that cork cells have a regular hexagonal prism shape, with dimension parameters measured directly from the cork sample under study (l, d_{width}, d_{height}, δ_{wall}), as shown in Table 1A. Additionally, the plasmodesmata diameter was measured and found to be of 100 nm. In the following analysis, n represents the number of cork cells along the gas flow direction (z).
(2) Supported on the data and discussion above, it was considered that gas transport occurs exclusively through the plasmodesmata. It was also considered that only the plasmodesmata aligned with the gas flow direction (z, see Fig. 11) contribute effectively to the gas transport. The plasmodesmata tortuosity, $\tau_{plasmodesmata}$ [−], and the number of plasmodesmata per cell, $\overline{n}_{plasmodesmata}$ [−], aligned with the gas flow direction, (z), were also determined based on the TEM images acquired.
(3) As the plasmodesmata are partially filled by a semipermeable material (to gases) to an unknown extent, different values were considered for equivalent diameter of plasmodesmata, varying between 95 and 40 nm.
(4) As the gas transport occurs exclusively through the plasmodesmata aligned with the gas flow direction, the transport model considers a hypothetical compact structure of cork (Fig. 11C), in which all cell walls perpendicular to the gas flow direction are standing back to back to each other. Therefore, the total effective thickness of the cork sample, $\delta_{compact}$ [m], is calculated as the number of cells along the gas flow direction, n [−], multiplied by the thickness of the cell wall, δ_{wall} [m].

The parameter n is easily calculated through Eq. (11):

$$n = \frac{\delta_{cork}}{d_{height}} \tag{11}$$

where δ_{cork} [m] is the thickness of the cork sample and d_{height} [m] is the diameter of the prism base along the gas flow direction.

The model developed also uses the molecular mass of the gas, M_i [g/mol], and the temperature as input variables. The model allows for estimating the gas diffusivities of natural cork, D_i [$m^2\ s^{-1}$] obtained through Eq. (10'):

$$D_i = \frac{\varepsilon_{compact} \times d_{plasmodesmata}}{3 \times \tau_{plasmodesmata}} \times \left(\frac{8RT}{\pi M_i}\right)^{1/2} \tag{10'}$$

The volumetric porosity of the compact structure of cork, $\varepsilon_{compact}$ [−], is defined as the ratio between the total void volume and the total volume, calculated though Eq. (12):

$$\varepsilon_{compact} = \frac{\overline{n}_{plasmodesmata} \times \pi/4 \times d^2_{plasmodesmata}}{l \times d_{width}} \tag{12}$$

where l [m] and d_{width} [m] are, respectively, the lateral prism length and the diameter of the prism base perpendicular to the gas flow direction (xy surface, at a certain z-value, see Fig. 11).

The estimation of the gas permeabilities are obtained with the values of the calculated gas diffusivities of natural cork, D_i [$m^2\ s^{-1}$], corrected for the overall thickness of the material, δ_{cork}, rather than the total effective thickness of the cork sample, $\delta_{compact}$.

Fig. 12 shows the experimental permeability of selected gases through the cork material plotted together with simulations obtained from the model developed in this work. The data required for estimating the gas permeabilities through cork are

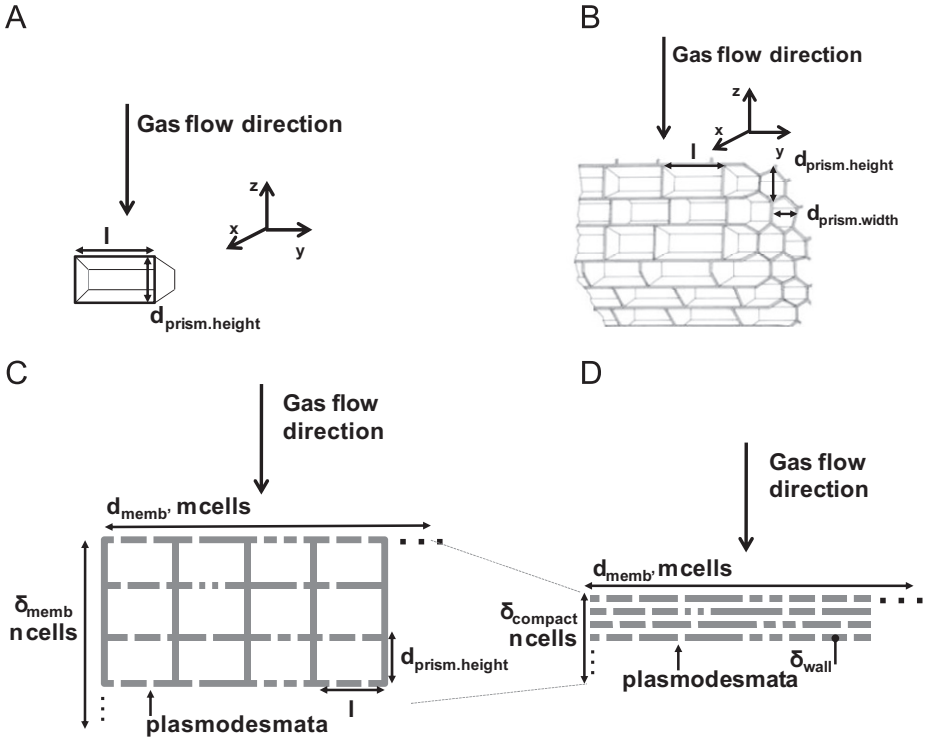

Fig. 11. Scheme of a cork cell (A). Scheme of the alveolar structure of the cross-section of the cork disk (B) and in 2-D (C) and the scheme of the hypothetical compact structure of cork in 2-D (D). Legend: n is the number of cork cells along z; m is the number of cork cells at a certain z-value (xy surface); d_{height} and d_{width} are the diameters of the prism base perpendicular to each other and l is the lateral prism length.

	Cork cells structure data Experimental measurements
δ_{memb}[m] x 10^3	2.1
l [μm]	50
d_{width} [μm]	29
d_{height} [μm]	32
δ_{wall} [μm]	1.(5)
$\tau_{plasmodesmata}$[-]	1
$\overline{n}_{plasmodesmata}$ [–]	3

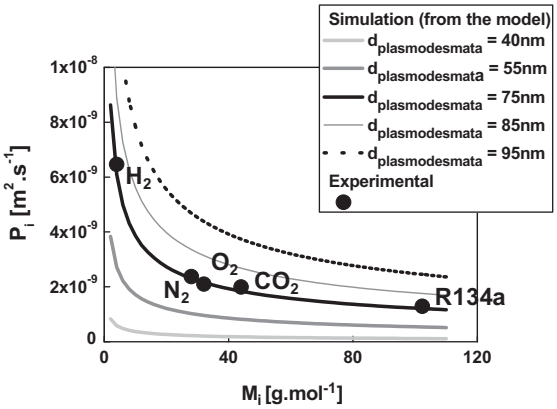

Fig. 12. Gas permeabilities through cork plotted *versus* the molecular weight of gas *i*. Symbols refer to experimental permeabilities of He, N_2, O_2, CO_2 and R134a to cork. Lines refer to simulated permeability values from the model using the cork morphological data, obtained experimentally in this work: δ_{cork}; average values of: *l*, d_{width}, d_{height} and δ_{wall} as in Table 1A; average values of $\tau_{plasmodesmata}$ and $\overline{n}_{plasmodesmata}$ as in Table 1B; and different values of equivalent diameter of plasmodesmata, $d_{plasmodesmata}$.

the morphology data of cork. The characterisation of cork was obtained by measuring the relevant geometric parameters of the natural material. The geometric parameters were measured considering the gas flow direction though the cork. In Fig. 12, the average values of the geometric parameters of the cell structure were considered, namely of the lateral prism length, *l*, the diameters of the prism base, respectively perpendicular and along the gas flow direction, d_{width} and d_{height} and the wall thickness of the cork cell, δ_{wall}, as shown in Table 1A. The average values of the parameters of the plasmodesmata were also considered, namely the tortuosity of the plasmodesmata, $\tau_{plasmodesmata}$ [−] and the number of plasmodesmata per cork cell along the gas flux direction, $\overline{n}_{plasmodesmata}$ [−], as in Table 1B.

A good agreement between estimated and experimental values of gas permeabilities through cork is observed, for an equivalent diameter of plasmodesmata of 75 nm, valid in a significant range of values of gas molecular mass. The fact that the best fit of the model with the experimental values corresponds to a plasmodesmata diameter of 75 nm is acceptable because it is lower than the diameter of real partially filled plasmodesmata (100 nm). Additionally, this proximity between experimental data and estimated results also proves that the transport mechanism present is indeed a Knudsen diffusion type.

Finally, the characterisation of cork enabled the calculation of the viscous contribution and of the molecular contribution to the total flux. The total flux of a gas *i* through a porous material, $J_{i,total}$ [mol m^{-2} s^{-1}], may be calculated through the sum of the different contributing types of fluxes, particularly by a diffusive transport (Knudsen molecular regime) and by convective transport (viscous regime), given by Eq. (13) [35]

$$J_{i,\text{total}} = -\frac{1}{RT} \times \left[D_i + \frac{k_i}{\mu_i} \times p \right] \times \frac{dp}{dx} \tag{13}$$

$$J_{i,\text{total}} = \frac{D_i \times p_{\text{feed}}}{\delta_{\text{compact}} \times RT} + \frac{k_i \times p_{\text{feed}}^2}{\delta_{\text{compact}} \times RT \times 2\,\mu_i} \tag{13'}$$

where D_i [m s^{-2}] is the diffusivity of a gas *i* through natural cork, calculated from Eq. (10'); μ_i [Pa s] is the dynamic viscosity of each gas and *k* [m^2] is the permeability of the porous material (in this case the hypothetically condensed cork structure), independent from the gas, which was calculated to be 2×10^{-21} m^2, through Eq. (14) [35]:

$$k_{\text{compact.cork}} = \frac{\varepsilon_{\text{compact}} \times d_{\text{plasmodesmata}}^2}{32 \times \tau_{\text{plasmodesmata}}} \tag{14}$$

Table 3
Percentage of the contribution of the viscous regime in relation to the total fluxes for each gas under study.

Gas	$J_{i,viscous}$[a]/$J_{i,total}$ (%)
He	1
O_2	4
N_2	4
CO_2	6
R134a	9.(7)

[a] Using dynamic viscosities at 20 °C, 1 bar [36].

where $\varepsilon_{compact}$ was calculated through Eq. (12), and as shown in Fig. 12 $\tau_{plasmodesmata}$ is 1 and $d_{plasmodesmata}$ is 75 nm, corresponding to the best fit of the model with the experimental values. The percentage of the contribution of the viscous regime in relation to the total flux for each gas studied is shown in Table 3. The contribution of viscous flow was found to be negligible (below 10%) for all selected gases, confirming that gas transport through cork follows predominantly a Knudsen molecular regime.

4. Conclusions

It was demonstrated that gas transport through cork follows a Knudsen molecular flow behaviour, as shown by the linear relation observed for gas permeability as a function of the $M_i^{-1/2}$ for the various gas *i* studied in this work. The driving force that regulates gas transport through cork is the gradient of partial pressure of a given gas, while convective transport represents a negligible contribution.

A model was developed based on the morphology of the cork cell structure, which was studied in this work and compared with the values reported in the literature. The model developed used the average values obtained from the morphological characterisation of cork, performed in this work. The methodology followed in developing this model may be applied to the study of gas transport in other complex natural materials.

The natural cork used in this work had no lenticular channels (macroscopic pores, hole spots, related to the quality of cork), which was confirmed experimentally. As a future work, it would be important to evaluate the effect of these lenticular channels, on gas permeability. The effect of different compressions of natural cork on gas transport should also be studied, specifically

at the compression conditions that natural cork is submitted to as a wine stopper.

Acknowledgments

The financial support of the Portuguese Foundation for Science and Technology is gratefully acknowledged (PTDC/EME-MFE/098738/2008). We thank Rita Teixeira for the TEM preparations and Isabel Miranda for help in TEM image analysis.

References

[1] A. Costa, H. Pereira, M. Madeira, Analysis of spatial patterns of oak decline in cork oak woodlands in Mediterranean conditions, Ann. For. Sci. 67 (2010) 204–213.
[2] V.B. Sousa, S. Leal, T. Quilhó, H. Pereira, Characterization of cork oak (*Quercus Suber*) wood anatomy, IAWA J. 30 (2) (2009) 149–161.
[3] S.P. Silva, M.A. Sabino, E.M. Fernandes, V.M. Correlo, L.F. Boesel, R.L Reis, Cork: properties, capabilities and applications, Int. Mater. Rev. 50 (6) (2005) 345–365.
[4] R.T. Teixeira, H. Pereira, Ultrastructural observations reveal the presence of channels between cork cells, Microsc. Microanal. 15 (2009) 539–544.
[5] M.A. Fortes, M.E. Rosa, H. Pereira, A Cortiça, Instituto Superior Técnico IST Press, 2004, pp. 18, 88.
[6] N. Cordeiro, M.N. Belgacem, A.J.D. Silvestre, C. Pascoal Neto, A. Gandini, Cork suberin as a new source of chemicals. 1. Isolation and chemical characterization of its composition, Int. J. Biolog. Macromol. 22 (1998) 71–88.
[7] P. Lopes, C. Saucier, Y. Glories, Nondestructive colorimetric method to determine the oxygen diffusion rate through closures used in winemaking, J. Agric. Food Chem. 53 (2005) 6967–6973.
[8] T. Karbowiak, R.D. Gougeon, J.B Alinc, L. Brachais, F. Debeaufort, A. Voilley, D. Chassagne, Wine oxidation and the role of cork, Food Sci. Nutrition. 50 (2010) 20–52.
[9] P. Lopes, C. Saucier, P.L. Teissedre, Y. Glories, Impact of storage position on oxygen ingress through different closures into wine bottles, J. Agric. Food Chem. 54 (2006) 6741–6746.
[10] A. Silva, M. Lambri, M.D. de Faveri, Evaluation of the performances of synthetic and cork stoppers up to 24 months post-bottling, Eur. Food Res. Technol 216 (2003) 529–534.
[11] S. Lequin, T. Karbowiak, L. Brachais, D. Chassagne, J.P. Bellat, Adsorption equilibria of sulfur dioxide on cork, Am J. Enol. Viticult 60 (2) (2009) 138–144.
[12] O. Anjos, H. Pereira, M.E. Rosa, Tensile properties of cork in the tangential direction: variation with quality, porosity, density and radial position in the cork plank, Mater. Des 31 (2010) 2085–2090.
[13] R.T. Teixeira, H. Pereira, Suberized cell walls of cork from cork oak differ from other species, Microsc. Microanal. 16 (2010) 569–575.
[14] H. Pereira, J. Graça, C. Baptista, The effect of the growth rate on the structure and compressive properties of cork, IAWA Bull. 13 (4) (1992) 389–396.
[15] H. Pereira, M.E. Rosa, M.A. Fortes, The cellular structure of cork from *Quercus Suber L.*, IAWA Bull. 8 (3) (1987) 213–218.
[16] H. Pereira, Cork: Biology, Production and Uses, Elsevier, 2007, pp. 33-52.
[17] H. Pereira, Chemical composition and variability of cork from *Quercus Suber* L., Wood Sci. Technol. 22 (3) (1988) 211–218.
[18] A. Costa, H. Pereira, Influence of cutting direction of cork planks on the quality and porosity characteristics of natural cork stoppers, Forest Syst. 19 (1) (2010) 51–60.
[19] S. Leal, V.B. Sousa, H. Pereira, Radial variation of vessel size and distribution in cork oak wood (*Quercus suber* L.), Wood Sci. Technol. 41 (4) (2007) 339–350.
[20] D.P. Faria, A.L. Fonseca, H. Pereira, O.M.N.D. Teodoro, Permeability of cork to gases, J. Agric. Food Chem. 59 (2011) 3590–3597.
[21] J. Sanchez, J.M. Aracil, Perméabilité gazeuse de différents obturateurs, Bull. l'OIV 71 (1998) 279–283.
[22] I. Pinnau, L.G. Toy, Gas and vapor transport properties of amorphous perfluorinated copolymer membranes based on 2,2-bistrifluoromethyl-4,5-difluoro-l,3-dioxole/tetrafluoroethylene, J. Membr. Sci. 109 (1996) 125–133.
[23] T.C. Merkel, V.I. Bondar, K. Nagai, B.D. Freeman, I. Pinnau, Gas sorption, diffusion, and permeation in poly(dimethylsiloxane), J. Polym. Sci., Part B: Polym. Phys 38 (3) (2000) 415–434.
[24] Y. Yampolskii, I. Pinnau, B.D. Freeman, Materials Sci. of Membranes for Gas and Vapor Separation, John Wiley & Sons, Ltd, 2006, pp. 6.
[25] 〈http://www.matbase.com/material/polymers/engineering/ptfe/properties〉.
[26] L.J. Gibson, M.F. Ashby, Cellular Solids: Structure and Properties, second ed., Cambridge University Press, Cambridge, 1997 453–467.
[27] I. Pinnau, L.G. Toy, Transport of organic vapors through poly(1-trimethylsilyl-1-propyne), J. Membr. Sci. 116 (1996) 199–209.
[28] A.Y. Alentiev, V.P. Shantarovich, T.C. Merkel, V.I. Bondar, B.D. Freeman, Y.P. Yampolskii, Gas and vapor sorption, permeation, and diffusion in glassy amorphous teflon AF1600, Macromolecules 35 (2002) 9513–9522.
[29] R.C. Reid, J.M. Prausnitz, B.E. Poling, The Properties of Gases & Liquids, McGraw-Hill, Inc., 1988, pp. 658–732.
[30] E.L. Cussler, Diffusion, Mass Transfer in Fluid Systems, second ed., Cambridge University Press, 1997, pp. 127–129 and 434–438.
[31] N.F.A. van der Vegt, V.A. Kusuma, B.D. Freeman, Basis of solubility *versus* T_C correlations in polymeric gas separation membranes, Macromolecules 43 (2010) 1473–1479.
[32] M.G. De Angelis, G.C. Sarti, F. Doghieri, Correlations between penetrant properties and infinite dilution gas solubility in glassy polymers: NELF model derivation, Ind. Eng. Chem. Res. 46 (2007) 7645–7656.
[33] M. Knudsen, Ann. Phys. (Leipzig) 28 (1909) 75.
[34] J.M. Lafferty, Foundations of Vacuum Science and Technology, John Wiley & Sons, Inc., 1998, pp. 81–86.
[35] T. Zivkovic, N.E. Benes, H.J.M. Bouwmeester, Gas transport efficiency of ceramic membranes: comparison of different geometries, J. Membr. Sci. 236 (2004) 101–108.
[36] Site of National Institute of Standards and Technology 〈http://webbook.nist.gov〉.